Renewable Energy 268 (2026) 125809



Contents lists available at ScienceDirect

Renewable Energy

journal homepage: www.elsevier.com/locate/renene

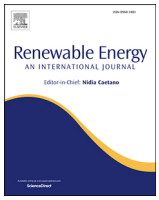



Unlocking the future of solar PV in Europe: high-resolution supply curves for decarbonizing the energy sector

Lucrezia Manservigi [a,*], Giulia Anna Maria Castorino [a], Pier Ruggero Spina [a], Mauro Venturini [a], Miguel Gonzalez-Salazar [b]

[a] Dipartimento di Ingegneria, Università degli Studi di Ferrara, Italy
[b] Institute for Sustainable Energy Systems (INSYS), Technical University of Applied Sciences Würzburg-Schweinfurt, Germany

ARTICLE INFO

Keywords:
Solar energy modeling
Scenario analysis
Renewable energy economics
Energy transition
Energy system decarbonization

ABSTRACT

Solar photovoltaics (PV) is a strategic technology, as it facilitates achieving net-zero emissions by 2050 while offering lower energy costs than competing renewable technologies. Its cost-effective deployment requires accurate projection of future supply curves, which unlock the relationship between power generation and levelized cost of electricity (*LCOE*) across time and space.

This paper develops a robust and generalizable methodology for deriving solar PV supply curves at high spatial resolution, integrating efficiency and cost of PV panels, geographic characteristics and ambient conditions. First, the methodology is validated against historical data; then, it is applied to project solar PV supply curves for the entire Europe and for six representative countries under three different scenarios for 2030 and 2050.

The results show that the maximum capacity to be installed in 2030 in Europe will be 3.5 TW, while it will be 4.8 TW in 2050. Correspondingly, *LCOE* is expected to be 22-62 USD/MWh in 2030 and 15-44 USD/MWh in 2050, depending on scenario assumptions. These findings provide essential inputs for policymakers and energy modelers, thus enabling the integration of country-specific solar PV supply curves into country energy plans. This will support more accurate and spatially resolved planning pathways towards achieving both cost-effective decarbonization and long-term climate targets.

Nomenclature

A	area [m^2]
a	availability [−]
C	capacity [kW]
CAPEX	capital expenditure [USD]
DR	degradation rate [−]
k	Constant
IC	installed costs [USD/kW]
LCOE	levelized cost of electricity [USD/kWh]
N	number [−]
O&M	operation and maintenance costs [USD/kW]
OPEX	operational expenditure [USD]
PG	yearly power generation [kWh/year]
R	Earth radius [km]
r	discount rate [−]
SDSR	surface downwelling shortwave radiation [W/m^2]
T	temperature [°C]
t	time [h]
WS	wind speed [m/s]

(*continued on next column*)

(*continued*)

γ	temperature coefficient [$°C^{-1}$]
Δ	range or variation
η	efficiency [−]
λ	longitude [°]
φ	latitude [°]
Subscripts	
c	Centroid
cell	PV cell
gc	grid cells
f	Factor
GC	ground coverage
LC	land cover
m	Module
PL	protected land
PR	performance ratio
s	suitable land
SC	standard conditions
TS	time stamp
UL	unsuitable land

(*continued on next page*)

* Corresponding author.
E-mail address: lucrezia.manservigi@unife.it (L. Manservigi).

https://doi.org/10.1016/j.renene.2026.125809
Received 20 May 2025; Received in revised form 15 April 2026; Accepted 15 April 2026
Available online 18 April 2026
0960-1481/© 2026 The Authors. Published by Elsevier Ltd. This is an open access article under the CC BY license (http://creativecommons.org/licenses/by/4.0/).

(*continued*)

Superscript	
*	spatial resolution
Acronyms	
AC	ambient condition
CDS	Copernicus climate data store
DOPA	digital observatory for protected areas
IAM	integrated assessment model
PV	Photovoltaics

1. Introduction

Climate change is a challenge with profound impacts on ecosystems, human societies and economies. Limiting average temperature increase below 1.5 °C with respect to pre-industrial levels requires (i) 45 % reduction in greenhouse gas emissions by 2030 compared to 2010 and (ii) achieving net-zero emissions by 2050 [1]. To address this urgency, through the European Green Deal, the EU has committed to a 55 % reduction in emissions from 1990 levels by 2030 and to achieve net-zero emissions by 2050 [2]. Realizing these goals requires substantial transformation of EU energy system, by shifting away fossil fuels towards low- and zero-carbon energy sources, as well as increased reliance on electricity and alternative energy carriers [2].

Solar photovoltaics (PV) is becoming increasingly important for cost-effective decarbonization, with the potential to achieve 10 % of the emission reductions needed to limit warming below 1.5 °C increase [3]. Driven by policy, societal pressure, low interest rates, and cost reductions, solar PV has experienced rapid growth [4]. Between 2013 and 2023, the solar PV installed capacity has increased 12-fold (1.7 TW), accounting for 18 % of the global installed capacity [5]. In the EU, solar PV is expected to become a cornerstone of energy transition. According to a European Commission study, solar PV capacity is projected to grow from 104 GW in 2018 to 310–374 GW by 2030 and 465–1060 GW by 2050 to meet Green Deal targets [6]. This expansion would enable solar PV to supply 12–14 % of total electricity. Achieving this will require substantial investments, not only in solar technology, but also in enhancing national and regional grid interconnections, expanding energy storage systems, electrifying demand, and advancing green hydrogen production to balance intermittent renewables [6].

In energy-system analysis, supply curves are a standard tool to represent how cumulative deployable potential increases with cost, considering resource quality, performance, and technical, economic or environmental constraints [7]. In the case of photovoltaics, differences in solar resource, ambient conditions, and land availability translate into variation in energy yield and levelized cost. The resulting supply curves are cost-potential relationships that inform energy planning, scenario analysis, and model-based assessments of future PV deployment [7], rather than prescribing land-use decisions. By translating spatial heterogeneity into marginal cost escalation, PV supply curves enable a transparent assessment of how much solar generation can be deployed below given cost thresholds and how this evolves over time.

In the particular context of PV, supply curves are addressed in fundamentally different ways across the existing studies. Most existing studies construct techno-economic PV supply curves by using geographic information system (GIS) data, linking cumulative PV potential to levelized generation costs at regional or national scale.

These analyses typically focus on physical potential, irradiance heterogeneity, land or rooftop availability, and assumed technology costs, and are often conducted as single-region case studies or within specific policy contexts, such as feed-in tariff (FIT) design. GIS data were used to construct PV supply curves in studies [3,8]. Study [3] examined 26 regions worldwide, including Africa, Australia, and South America, whereas [8] focused on Fujian Province, China. Study [5] developed PV supply curves for Argentina, Brazil, Chile, and Mexico for the years 2014 and 2025, based on technological and economic parameters. Study [9] derived current PV supply curves for the contiguous United States (CONUS) by incorporating economies-of-scale cost curves for solar PV. Finally [6], constructed PV supply curves for Taiwan and analyzed their relationship with FIT levels.

Other studies use the notion of a supply curve to analyze how PV affects electricity markets through the merit order, focusing on price formation and price volatility rather than on deployable PV potential. These works examine how increasing PV penetration reshapes the market supply curve and modifies clearing prices and variance in wholesale electricity markets, examples include [10,11]. A further group of papers develop PV supply curves within optimization or integrated assessment models (IAMs), where they serve as inputs to represent resource heterogeneity, drive endogenous deployment, or avoid corner solutions in cost-minimizing models. In these cases, the supply curves are usually model-internal and not intended as standalone, transparent products. Examples include the regional cost-supply curves for rooftop PV in IMAGE [4] and the use of PV supply curves in a South Korea's TIMES model [12]. Additional studies use the term supply curve in a broader market or socio-economic sense, such as housing or rooftop rental markets, congestion management, or transactive energy coordination, rather than as PV cost-potential curves. For example, transitioning from illegal rooftop rentals to solar PV adoption [13], and an aggregator-led market where a supply curve is formed to manage congestion in PV multi micro grids [14].

Despite substantial progress, three key gaps remain across studies. First, standalone, Europe-wide PV cost-potential supply curves at high spatial resolution are still scarce, limiting their direct use in energy planning and modeling. Second, many existing studies rely on simplified representations of spatial heterogeneity and technology evolution, which limits the correct shaping of the slope and curvature of supply curves over time, as a function of PV costs and performance. Third, external validation is often limited, with supply curves rarely benchmarked simultaneously against historical levelized cost of electricity (*LCOE*) ranges and observed deployment levels.

This study addresses these gaps by developing a general and transparent methodology to derive PV cost-potential supply curves for a given territory that jointly accounts for technology efficiency, investment costs, geographic characteristics, and ambient conditions. Europe is used as a comprehensive case study. The methodology is first validated against historical data and subsequently applied to project high-resolution PV supply curves for the entire Europe as well as six representative countries for 2030 and 2050 under three distinct scenarios.

The key contributions of this study are summarized below:

- Development and validation of a novel methodology for deriving solar PV supply curves. This approach integrates simulations of *LCOE* and PV capacity, which are rigorously benchmarked against actual values in Europe in the period 2010-2022.
- Projection of solar PV supply curves for 2030 and 2050, by considering both *LCOE* and PV capacity, unlike previous studies that treated these aspects separately. This paper provides country-level and EU-wide curves, thus offering practical guidance for policy makers and investors.
- Quantitative assessment of the key drivers that shape solar PV supply curve, including (i) ambient conditions, (ii) cost, (iii) solar PV efficiency, and (iv) rate of developable area for PV deployment.

From a more general perspective, the results documented in this paper can be used to feed regional IAMs and equilibrium models, support medium- and long-term energy and economic analyses, as well as country-level evaluations about solar PV cost-effectiveness compared to other energy technologies. This study also aims to contribute to the strategic planning necessary to accelerate Europe's transition to a low-carbon energy system.

2. Methodology

The methodology developed in this paper (outlined in Fig. 1) allows deriving PV supply curves for a given territory, by relating the *LCOE* to capacity, which is proportional to the developable area. Capacity maximum value represents the photovoltaic potential of a territory and differs from the installed capacity that, instead, refers to the *actual* value deployed within a given territory. In summary, supply curves allow (i) assessing the maximum available capacity of a given territory and (ii) identifying the most suitable territories for PV deployment.

In the developed methodology, the target territory (e.g., region, country or continent) is divided into N_{gc} grid cells. Each cell is characterized by means of four input categories listed in Table 1. This enables the calculation of (i) PV capacity (C_{PV}), and (ii) *LCOE* of *each cell*.

Land cover classes (e.g., grassland or urban area) and ambient conditions (i.e., surface downwelling shortwave radiation (*SDSR*), air temperature (*T*), and wind speed (*WS*)) are extracted from the Copernicus Climate Data Store (CDS) [15]. Additional ambient conditions (e.g., humidity, precipitation, and snow cover) are not considered. Information on protected areas is inferred from the Digital Observatory for Protected Areas (DOPA) Explorer [16]. It is worth noting that the resolution (i.e., cell dimension) of data extracted from Ref. [15] is not uniform. Land cover data are provided at a fine resolution of $\Delta\varphi^* \times \Delta\lambda^*$ is $0.0028^\circ \times 0.0028^\circ$ (approximately 309 m × 309 m), whereas ambient conditions are available at a coarser resolution of $\Delta\varphi \times \Delta\lambda = 0.25^\circ \times 0.25^\circ$ (approximately 28 km × 28 km). Instead, a customized grid with resolution of approximately 309 m × 309 m is created to associate the actual rate of protected area with each cell. For the sake of clarity, the superscript "*" labels the variables that refer to the data with the finer resolution.

For *each cell* of the grid, the corresponding solar capacity C_{PV} and *LCOE* is calculated as shown in Fig. 2.

First, cell area (also named land cover area A^*_{LC}) is evaluated by using Eq. (1), where *R* is the Earth radius

($R = 6371$ km), and φ^*_c is the latitude of cell centroid (i.e., grey circle in Fig. 1).

$$A^*_{LC} = \left(\frac{\pi}{180}\cdot R\cdot 1000\right)^2 \cdot \Delta\varphi^* \cdot \Delta\lambda^* \cdot \frac{1}{\cos\varphi^*_c} \quad (1)$$

Cell area A^*_{LC} is only partially suitable for installing PV panels [17]. Land cover classes such as forests, shrub lands, wetlands, permanent snow or ice, and water bodies are considered unsuitable (A^*_{UL}), as well as protected areas (A^*_{PL}) [18]. In these cases, the suitable area (A^*_s) is null. In contrast, areas labeled as cropland, grassland, barren land, and desert

Table 1
Methodology inputs.

Input categories	Name
Geographic inputs	Land cover class (A^*_{UL})
	Protected areas (A^*_{PL})
	Availability factor (a^*_f)
Ambient conditions	Surface downwelling shortwave radiation (*SDSR*)
	Air temperature (*T*)
	Wind speed (*WS*)
Performance inputs	Module efficiency (η_m)
	Performance ratio (η_{PR})
	Ground coverage (η_{GC})
Economic inputs	Installed cost (*IC*)
	Operation and management cost (*O&M*)
	Discount rate (*r*)

are suitable for the installation of solar PV. Unlike studies [18,19], we also exploit urban areas, as rooftop solar PV may be necessary for addressing the decarbonization goals [20]. Protected areas A^*_{PL} are calculated by multiplying the share of protected areas (derived from Ref. [16]) by the land cover area A^*_{LC}. Equation (2) defines the suitable land (A^*_s).

$$A^*_s = A^*_{LC} - A^*_{UL} - A^*_{PL} \quad (2)$$

Only a small fraction of the suitable land area A^*_s is available for solar PV, as it may also be exploited for other uses [19]. Eq. (3) is used to calculate the area available for the installation of solar PV (A^*_{PV}):

$$A^*_{PV} = a^*_f \cdot A^*_s \quad (3)$$

where a^*_f is the availability factor, which ties land exploitation to land cover class and country (i.e., developing or industrialized).

It must be noted that, at this stage, cell dimension is standardized at approximately 28 km × 28 km, thus obtaining high-resolution supply curves while reducing the computational effort. To achieve this, multiple cells (in the order of 10^4) representing the available PV area A^*_{PV} (red rectangles in Fig. 1) are aggregated into a uniform resolution area (blue rectangle in Fig. 1).

Power generation *PG* is calculated by means of Eq. (4). It should be noted that PV degradation is neglected. *PG* depends on surface downwelling shortwave radiation (*SDSR*) that, in Ref. [15], is the amount of solar radiation that reaches a horizontal PV (i.e., the tilt angle is null) that has fixed orientation. The *SDSR* is corrected to account for temperature effects by using: (i) a temperature coefficient γ equal to $-0.005\ ^\circ C^{-1}$ for monocrystalline silicon PV panels [21], (ii) the PV cell

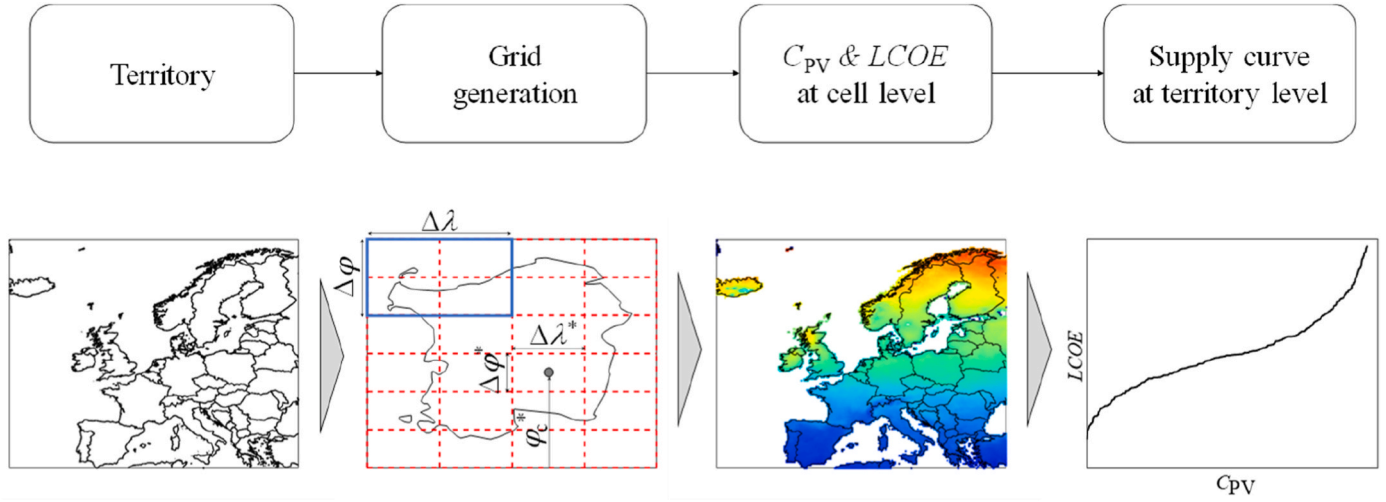

Fig. 1. Methodology for deriving the supply curves.

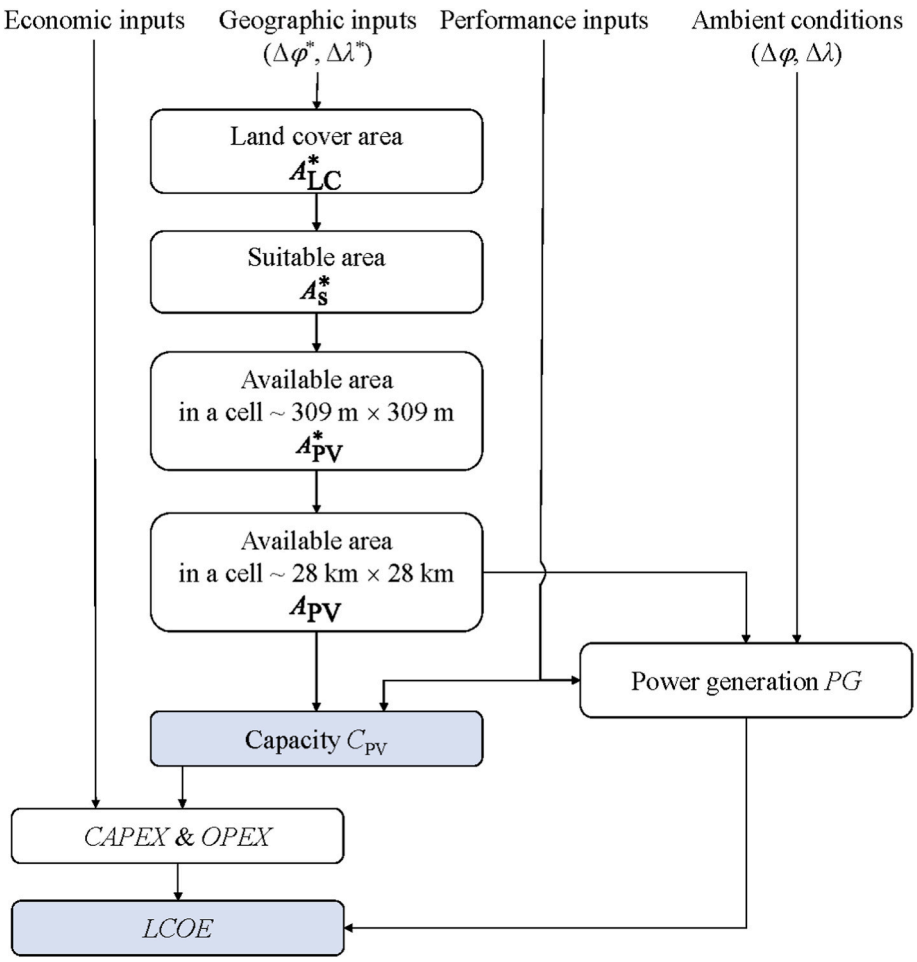

Fig. 2. Methodology workflow (cell level).

temperature T_{cell}, and (iii) temperature at standard conditions T_{SC}, which is 25 °C. PV cell temperature T_{cell} is influenced by air temperature (T), $SDSR$ and wind speed (WS), as shown in Eq. (5), where $k_1 = 4.3$ °C, $k_2 = 0.943$, $k_3 = 0.028$ °C m^2/W, and $k_4 = -1.528$ °C s/m [21].

Corrected $SDSR$ is multiplied by the time interval Δt, available area A_{PV} and solar PV efficiency η_{PV}. As shown in Eq. (6), solar PV efficiency η_{PV} is given by the product of (i) the efficiency of the individual solar module (η_m); (ii) the performance ratio η_{PR}, which accounts for system conversion efficiency from module output to useable electricity; and (iii) the share of the area actually covered by PV cells (η_{GC}) [18]. Power generation PG during j-th year in kWh/year is obtained by summing all N_{TS} contributions.

$$PG_j = \sum_{i=1}^{N_{TS}} \frac{SDSR_i \cdot \left[1 + \gamma \cdot \left(T_{cell,i} - T_{SC}\right)\right]}{1000} \cdot \Delta t \cdot \eta_{PV} \cdot A_{PV} \tag{4}$$

$$T_{cell,j} = k_1 + k_2 \cdot T + k_3 \cdot SDSR_j + k_4 \cdot WS_j \tag{5}$$

$$\eta_{PV} = \eta_m \cdot \eta_{PR} \cdot \eta_{GC} \tag{6}$$

The PV capacity C_{PV} of each cell of the grid is the maximum power output (expressed in kW) under standard conditions [22], by assuming $SDSR_{SC} = 1000$ W/m^2 in Eq. (7).

$$C_{PV} = \eta_{PV} \cdot \frac{SDSR_{SC}}{1000} \cdot A_{PV} \tag{7}$$

Then, the levelized cost of electricity ($LCOE$) [USD/kWh] is calculated for each grid cell by using Eq. (8). $LCOE$ is defined as the net present value of all costs over plant lifetime divided by the discounted electricity generation [23]. It represents the electricity price needed to cover all lifetime costs, including a return on the invested capital equal to the discount rate r.

The numerator of Eq. (8) accounts for both capital expenditures ($CAPEX$) and operation and maintenance costs ($OPEX$). $CAPEX$ is allocated in one year and is proportional to installed solar PV capacity C_{PV} and installed cost IC (see Eq. (9)). $CAPEX$ includes hardware costs (e.g., modules, inverters, control systems), installation, and soft costs (e.g., margin and financing costs) [24]. $OPEX$ is obtained by multiplying PV capacity by annual $O\&M$ costs (see Eq. (10)), which cover logistics, labor, and spare parts, and is applied over plant entire lifetime of N years.

$$LCOE = \frac{CAPEX + \sum_{j=1}^{N_{year}} \frac{OPEX_j}{(1+r)^j}}{\sum_{j=1}^{N_{year}} \frac{PG_j}{(1+r)^j}} \tag{8}$$

$$CAPEX = IC \cdot C_{PV} \tag{9}$$

$$OPEX = O\&M \cdot C_{PV} \tag{10}$$

The supply curve unlocks the relationship between cumulative PV capacity (C_{PV}) and $LCOE$. Each j-th cell of the territory (N_{gc} in total) is characterized by two parameters: $LCOE$ and PV capacity. The supply curve is constructed by first sorting the N_{gc} cells in ascending order of $LCOE$. Thus, the first point of the supply curve corresponds to the cell with the lowest-cost. Each subsequent j-th point represents the $LCOE$ of the j-th cell (in ascending order) plotted against the cumulative PV

capacity obtained by summing all C_{PV} values up to the j-th cell. In this way, the upper bound of the supply curve corresponds to the maximum available capacity of a given territory.

3. Case study

Territory. The methodology described in Section 2 is applied to the territory spanning latitudes from −22° to 32°, and longitudes from 36° to 73° (see Fig. 3). This includes the EU-27 (excluding Cyprus), eight EU candidate or potential candidate countries (Albania, Bosnia and Herzegovina, Moldova, Montenegro, North Macedonia, Serbia, and part of Turkey and Ukraine), the northern part of Algeria and Tunisia, and seven additional countries (Belarus, Iceland, Liechtenstein, Norway, a small fraction of Russia, Switzerland, and UK). In total, forty-three countries are considered, most of which belong to Europe (either politically or geographically). The supply curves derived in this paper refer to both the entire region, and six countries currently leading in PV capacity (France, Germany, Italy, The Netherlands, Spain, and UK) [25].

Geographic inputs. As previously mentioned, unsuitable land A^*_{UL} and protected areas A^*_{PL} are derived from the Copernicus Climate Data Store (CDS) [15] and the Digital Observatory for Protected Areas (DOPA) Explorer [16], respectively. In CDS, each cell of the grid is labeled with one land cover class available from 1992 to 2022. However, land cover remained unchanged in 96.5 % of the cells over this period. Thus, in this study, the land cover class of each cell is assumed to be constant and equal to the value in year 2020. The considered territory accounts for more than 50 ecoregions (Fig. 3), with protected area shares as high as 78 % (i.e., forests in Corsica).

According to Eq. (3), the available area for PV installation A^*_{PV} depends on the availability factor a^*_f, which is highly uncertain [18]. To overcome this issue, the current paper investigates three scenarios, denoted as "low a^*_f", "medium a^*_f" and "high a^*_f" (Table 2). The value of a^*_f depends on technology, land cover class (e.g., cropland, grassland, barren land, desert, urban) and country (developing or industrialized). Values reported in Table 2 refer to industrialized countries.

The availability factor a^*_f for cropland, barren area, grassland, and desert was derived from studies [18,26]. Cropland is characterized by the lowest availability factor as the portion of farmland that is converted to PV is usually low. Instead, desert has the highest availability factor, as shown in Ref. [27]. The availability factor in urban areas is derived by excluding grasslands and area covered by trees and water [28], and by assuming that 66 % of rooftop areas can be actually exploited [29]. The difference across land cover classes is mainly evident in the "low a^*_f" scenario, where desert land is 20 times more attractive than cropland, but such a difference reduces in the "high a^*_f" scenario. Notably, a^*_f values are scenario-dependent, but remain constant over time.

Ambient conditions. The key ambient conditions (*SDSR*, *T* and *WS*) are derived from the CDS [15], which provides data from 1951 to 2100. Historical conditions are derived from re-analyses [30], which combine observational data (from weather stations, satellites, balloons, aircraft, etc.) with numerical weather models to ensure consistency. Future projections are generated by using global and regional climate models. Global climate models simulate climate system responses to greenhouse gas concentrations, while regional models refine these projections for specific geographic territories. The study [31] compared five different combinations of global and regional models, demonstrating that they were on average equivalent. Thus, this paper adopts the combination of NorESM1-M (global climate model) and HIRHAM5 (regional climate model). Projections are made under the Representative Concentration Pathway (RCP) 4.5, which assumes a global temperature increase of 2 °C to 3 °C above pre-industrial levels by 2100 [32]. The highest time granularity available in CDS is used, i.e., 3 h.

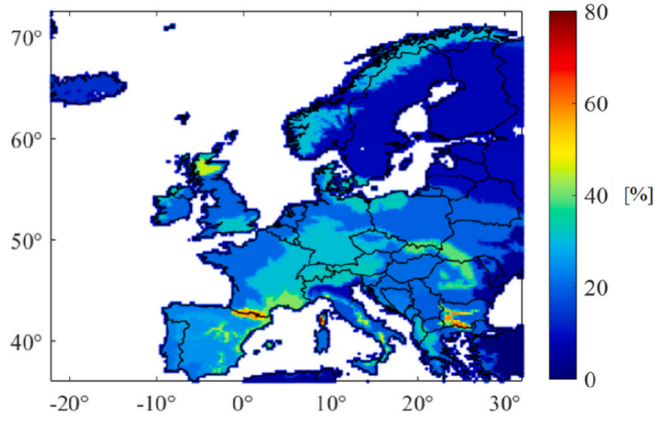

Fig. 3. Rate of protected areas inferred from the DOPA Explorer [16].

Table 2
Availability factors a^*_f for industrialized countries.

	Scenario		
	Low a^*_f	Medium a^*_f	High a^*_f
Cropland	0.1 %	0.5 %	2.0 %
Barren land	0.5 %	1.0 %	3.0 %
Grassland	0.5 %	1.0 %	3.0 %
Desert	2.0 %	5.0 %	8.0 %
Urban area	1.0 %	2.5 %	4.0 %

Performance inputs. According to Eq. (6), solar PV efficiency is the product of η_m, η_{PR}, and η_{GC}, which are expected to vary over years, especially the module efficiency η_m [18]. System losses are accounted for by means of η_{PR} and also depend on installation year. In agreement with [24], solar PV system operates for 25 years, during which the efficiency η_{PV} is calculated in the year of installation. The efficiency value is calculated for the first year of operation by linearly interpolating data from Table 3 [18].

Economic inputs. Fig. 4 shows the installed cost *IC* for Europe and the six considered countries (France, Germany, Italy, The Netherlands, Spain, and UK) from 2010 through 2050. For the 2010-2022 period, a single *IC* value, calculated as the average across the six countries, is applied across all grid cells to estimate the European *LCOE*. In contrast, the national analyses use each nation's specific average.

As shown in Fig. 4, installed costs *IC* reduced over time, by up to 86 % between 2010 and 2022, and are expected to decline further, largely independent of the decarbonization pathway (e.g., Stated Policies Scenario, Announced Pledges Scenario, or Net Zero Emissions by 2050 Scenario) [33]. This paper adopts projections from the Stated Policies Scenario, where *IC* is expected to reduce by 29 % from 2030 to 2050 [33]. While *IC* varied considerably across countries until 2014, more uniform values are being observed in the last decade. Thus, we assume a uniform *IC* across all European countries in 2030 (480 USD/kW) and 2050 (340 USD/kW); these costs decline due to an increase in the global cumulative installed capacity over time, i.e., learning curve effects.

The installed cost *IC* is accounted for in the year of installation, while *OPEX* is assumed to be equal to 1.9 % of *CAPEX* [24]. The discount rate *r* varies over years as shown in Table 4 [24]. A 25-year operational lifetime is assumed for all solar PV systems [24].

Table 3
Performance inputs [18].

	η_m	η_{PR}	η_{GC}
2010	16.0 %	75.0 %	20.0 %
2030	24.0 %	80.0 %	23.0 %
2050	29.5 %	80.0 %	26.5 %

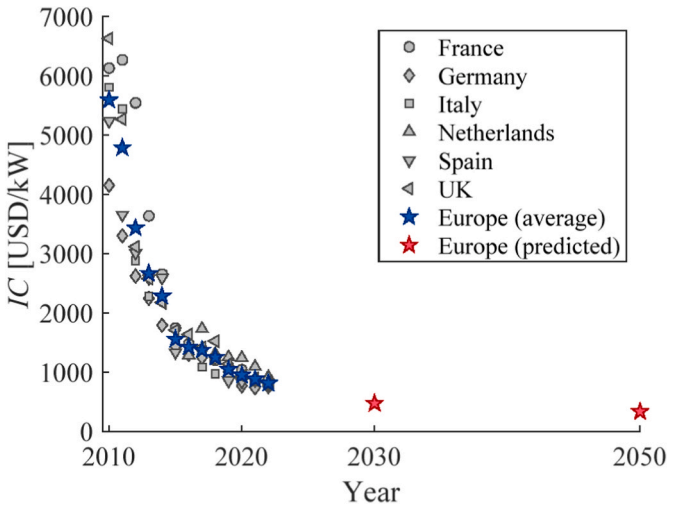

Fig. 4. Installed cost *IC*.

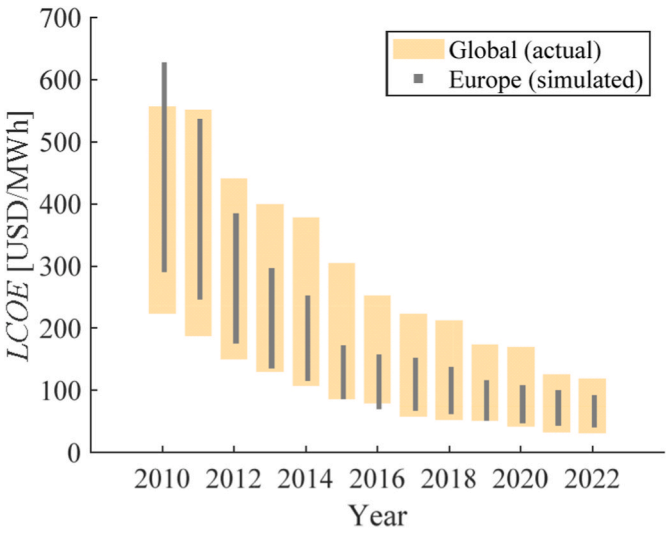

Fig. 5. Actual (yellow bars) *vs.* simulated (grey bars) *LCOE*.

4. Results and discussion

In this Section, we first present the validation of the methodology developed in Section 2 and then we report and discuss the projected supply curves for 2030 and 2050.

Both validation and projection are conducted at the European level (covering forty-three countries) and at country level for France, Germany, Italy, The Netherlands, Spain, and UK.

Validation of the methodology. Validation results are shown in Fig. 5 (European level) and Fig. 6 (country level). Fig. 5 compares the *LCOE* simulated from 2010 to 2022 with actual global values taken from Ref. [24], by using the range between the fifth and ninety-fifth percentiles as made in Ref. [24]. These *LCOE* values are scenario-independent, as both PV costs (i.e., *LCOE* numerator) and power generation (i.e., *LCOE* denominator) are proportional to the availability factor (a_f^*).

It is worth highlighting that the actual *LCOE* (yellow bars) accounts for PV plants installed globally in each year, while the simulated values (grey bars) assume full utilization of available area A_{PV} in *all* grid cells.

The simulated *LCOE* values fall within the actual range for all years with the exception of 2010. In that year, slight exceedances occur only in few cells located in Iceland, Scandinavia, and Scotland, where the installation of PV panels is limited by low solar irradiance and high costs.

As expected, the decrease in installed cost over time (see Fig. 4) drove a significant reduction in *LCOE* from 2010 to 2022.

Fig. 6 presents the results for France, Germany, Italy, the Netherlands, Spain, and UK in 2020. For each country, Fig. 6 reports (i) the simulated supply curves for the scenarios "low a_f^*", "medium a_f^*", and "high a_f^*" (see Table 3), (ii) the actual average *LCOE* ($LCOE_{av}$) (red circle) [24], and (iii) the cumulative installed capacity C_{PV} by 2020 (dashed black line) [25].

As highlighted in Eqs. (3) and (7), a higher availability factor a_f^* leads to larger capacity C_{PV}. For clarity, the scale of Fig. 6 is limited to 100 GW for all countries. Fig. 6 proves that the simulated scenarios are in agreement with the actual capacity C_{PV} (dashed black line). Notably, the minimum and maximum *LCOE* values are the same across scenarios, as previously discussed. In addition, the actual average $LCOE_{av}$ falls within the range projected by the model.

These results confirm the robustness of the methodology: both the simulated *LCOE* range (Figs. 5 and 6) and capacity C_{PV} (Fig. 5) are in agreement with the actual data documented for the year 2020.

Fig. 6 also allows identifying the most plausible scenario for each country as well as evaluating whether the most suitable areas have been actually exploited for solar PV deployment. This can be inferred by comparing the position of the actual average $LCOE_{av}$ to the simulated supply curves. For example, France and The Netherlands have exploited the best areas for solar PV, as their $LCOE_{av}$ values align with the scenario "high a_f^*", while their actual capacities C_{PV} remain below the maximum (less than half in The Netherlands), meaning limited land exploitation. In contrast, Spain shows the opposite trend, as only a small fraction of suitable land has been exploited for solar PV (i.e., the $LCOE_{av}$ is on the left-hand side of the supply curve derived for the scenario "low a_f^*"). Finally, it can be observed that in Germany and the Netherlands, the installed capacity (dashed black line) exceeds the maximum available capacity estimated under the "low a_f^*" scenario. This suggests that a more intensive land use occurred in these countries, making the scenarios "medium a_f^*" and "high a_f^*" scenarios more representative of the actual deployment.

A further validation was performed to assess the reliability of the availability factors reported in Table 2. The actual installed capacity (derived from Ref. [34]) in each of the 107 Italian provinces in 2020 was compare to the maximum available capacity of each province estimated for the three scenarios (i.e., "low a_f^*", "medium a_f^*", and "high a_f^*"). The results indicate that 60 provinces exhibit land-use levels consistent with the low availability scenario (blue areas in Fig. 7), while 45 provinces show intermediate deployment, i.e., between the low and medium

Table 4
Economic inputs.

Year	*IC*		*O&M*	*r*	N_{years}
	FR, DE, IT, NL, ES, UK	Europe			
2010-2019	Yearly average value of each country (Fig. 4)	Yearly average value of the six *ICs* (Fig. 4)	1.9 %·*IC*	7.5 %	25
2020-2022				5 %	
2030	480 USD/kW			5 %	
2050	340 USD/kW				

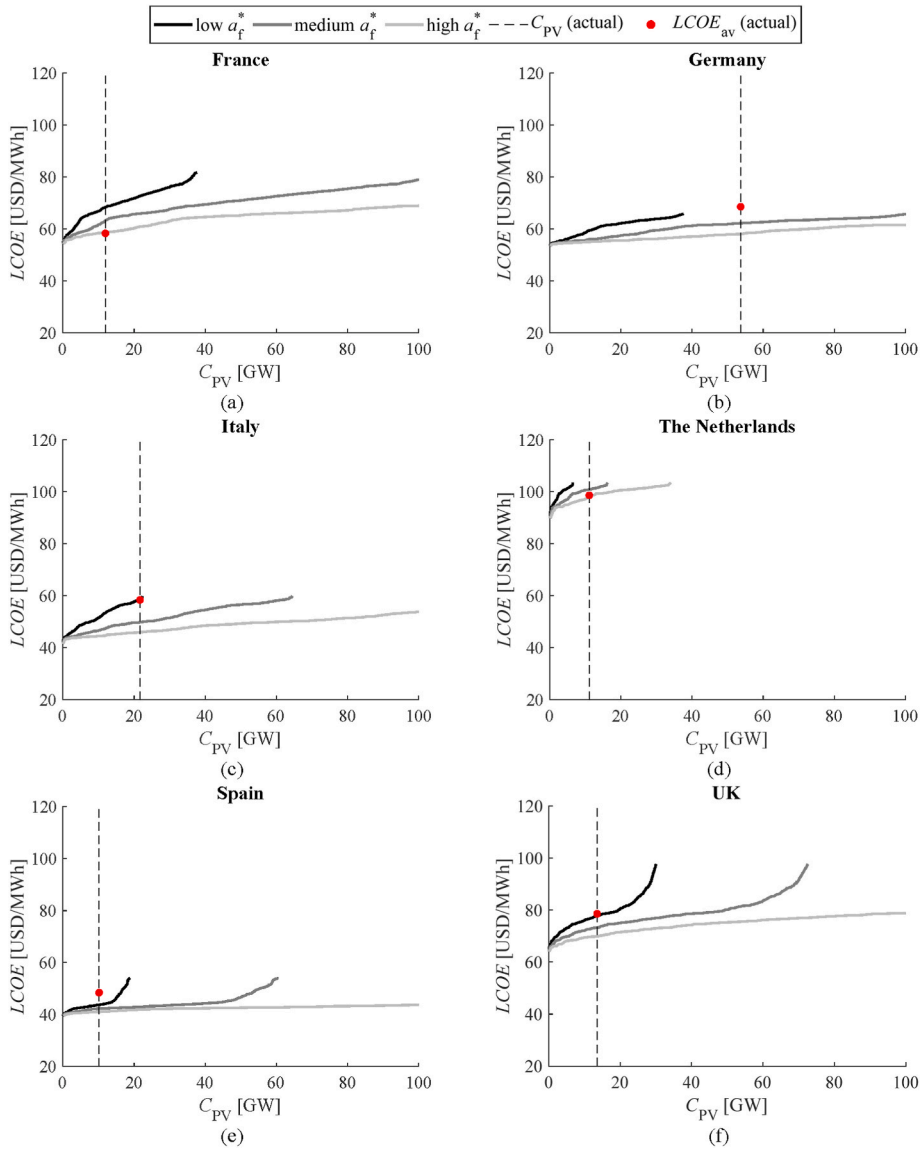

Fig. 6. Simulated supply curves in year 2020.

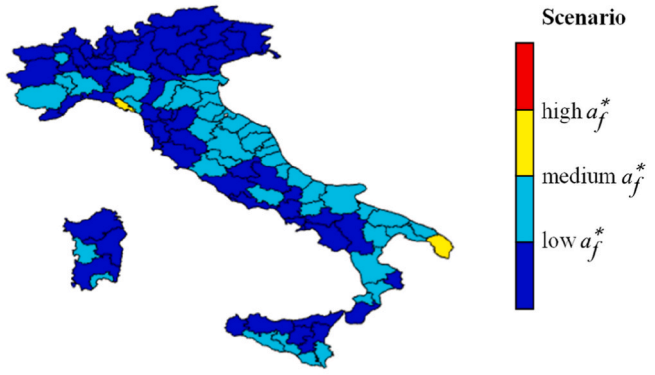

Fig. 7. Installed capacity in Italy in 2020 compared to the maximum available capacity estimated for the three scenarios "low a_f^*", "medium a_f^*", and "high a_f^*"

availability scenario (light-blue areas in Fig. 7). Finally, two provinces (yellow areas in Fig. 7) display land-use levels between the medium and high availability scenario. The most notable result is that no province exhibits land-use levels exceeding those predicted by considering the high availability scenario. These findings suggest that the availability factor values adopted in this study are robust.

Projection of the supply curves and discussion. Fig. 8(a) and 9(a) show the projected supply curves for Europe in 2030 and 2050, while Fig. 8(b) and 9(b) report the corresponding *LCOE* values. Overall, *LCOE* increases with latitude and is substantially independent of longitude.

From 2030 to 2050, *LCOE* is expected to decrease by about 30 %. The projected *LCOE* (i.e., 22–62 USD/MWh in 2030 and 15–45 USD/MWh in 2050) is consistent with the values reported in the literature [33] and shown in Table 5. These projections confirm that PV panels will offer the lowest *LCOE*, outperforming other renewable (e.g., wind) and non-renewable (e.g., nuclear) alternatives. In Europe, the maximum available capacity C_{PV} is projected to increase by 30-38 % from 2030 to 2050, depending on the scenario. This growth is not driven by the area suitable for PV installation (A_{PV}), but by a projected increase of 42 % in PV efficiency.

Under the high-availability scenario (assuming that available area A_{PV} is fully utilized), Europe's maximum available capacity C_{PV} could reach 3.5 TW in 2030, which is approximately six times the value required to reduce GHG emissions by 55 % [35], and 4.8 TW in 2050.

The decrease in *LCOE* and the increase in maximum available

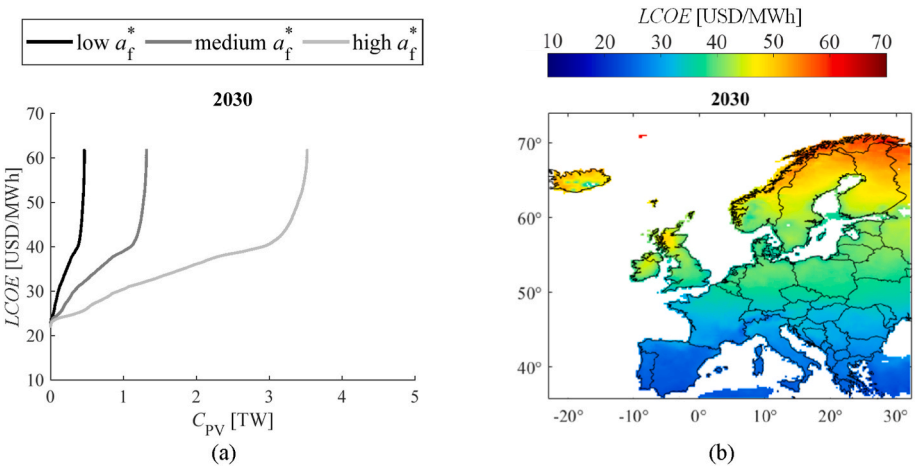

Fig. 8. Projected supply curves (a) and *LCOE* (b) in Europe in 2030.

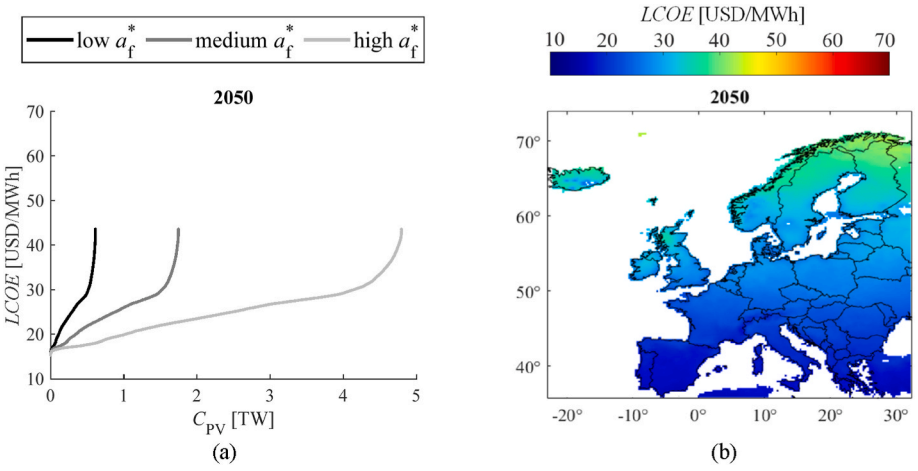

Fig. 9. Projected supply curves (a) and *LCOE* (b) in Europe in 2050.

Table 5
Average *LCOE* [USD/MWh] in the European Union [33].

	Year 2030	Year 2050
Solar PV	35	25
Wind onshore	55	50
Wind offshore	45	35
Nuclear power plant	135	125
Gas CCGT	260	n.a.

capacity C_{PV} over decades are driven by three factors: ambient conditions (ACs, i.e., *SDSR*, *T*, *WS*), installed cost (*IC*), and PV panel efficiency (η_{PV}). To determine the influence of each input, a sensitivity analysis is conducted (Fig. 10), focusing on the scenario "medium a_f^*" for 2020 and 2050 (black curves). The grey supply curves are obtained by individually updating each input from its 2020 value to its projected 2050 value, while holding the other two inputs constant at their 2020 levels. As shown, the variation in ambient conditions (grey dashed line) negligibly affects the future supply curves. This result agrees with other studies (e.g., Refs. [21,34,36]), which estimate that climate change will slightly affect solar power production is Europe. The installed cost *IC* (grey dotted line) determines the intercept of the supply curve, and thereby the minimum *LCOE*.

The slope of the curve is affected by both the installed cost and PV efficiency η_{PV}, but it is mainly driven by *IC*. Given the decrease in *IC* and the increase in η_{PV}, the supply curve becomes less steep over time. The

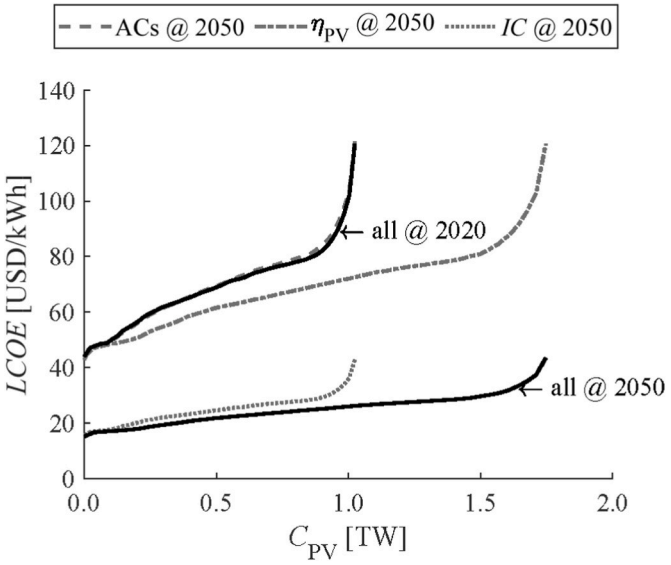

Fig. 10. Sensitivity analysis (scenario "medium a_f^*").

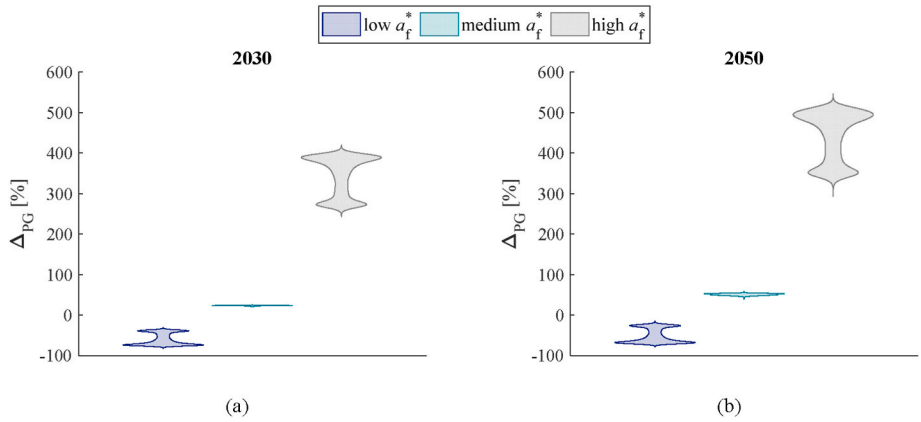

Fig. 11. Variation in yearly power generation *PG* with respect to scenario "medium a_f^*" in 2020.

impact of PV efficiency η_{PV} (grey dotted-dashed line) is substantial. An increase in efficiency raises the power generation (see Eq. (4)), maximum available capacity C_{PV} (see Eq. (7)) and reduces *LCOE*.

The associated increase in the annual power generation (Δ_{PG}) is shown in Fig. 11, by using the scenario "medium a_f^*" in 2020 as benchmark. Compared to 2020, PV efficiency increases by 25 % in 2030 and 88 % in 2050, leading to proportional increases in power generation under both scenarios "medium a_f^*" and "high a_f^*" (Fig. 11). In scenario "high a_f^*", power generation increases further because of the improvement of both solar PV efficiency and availability factor a_f^*, which quadruples. However, an increase in solar PV efficiency does not guarantee higher *PG* if land availability remains limited, as demonstrated by the scenario "low a_f^*".

The supply curves shown in Fig. 8(a) and 9(a) are used as benchmarks to assess the influence of PV degradation on *LCOE* and, consequently, supply curves. For this purpose, Eq. (4) was modified as made in Ref. [37], to account for a degradation rate (*DR*). Two values of degradation rates were considered, i.e., 0.7 %/year and 1.5 %/year [37]. As expected, PV degradation shifts the supply curves toward higher *LCOE* values as power output decreases. Thus, the higher the degradation rate, the higher the *LCOE*. A degradation rate of.

0.7 %/year makes *LCOE* increase by approximately 7 %, while a *DR* of 1.5 %/year makes *LCOE* increase by about 15 %. These outcomes apply independently of the considered availability factor (low, medium, high) and year (2030 or 2050). Thus, a rule of thumb can be inferred, i.e., *LCOE* relative increase over a lifetime of 25 years is approximately ten times the yearly degradation rate.

Fig. 12 shows the ratio of land cover area that can be actually exploited (A_{PV}/A_{LC}), by identifying areas with the greatest potential for largest solar PV deployment in Europe. Under the scenario "medium a_f^*" (Fig. 12), this ratio is usually below 1 %, with the exception of some urban cells where it is up to 1.6 %. These values are lower than the maximum availability factor a_f^* reported in Table 2, as A_{PV} aggregates multiple cells with different land cover classes.

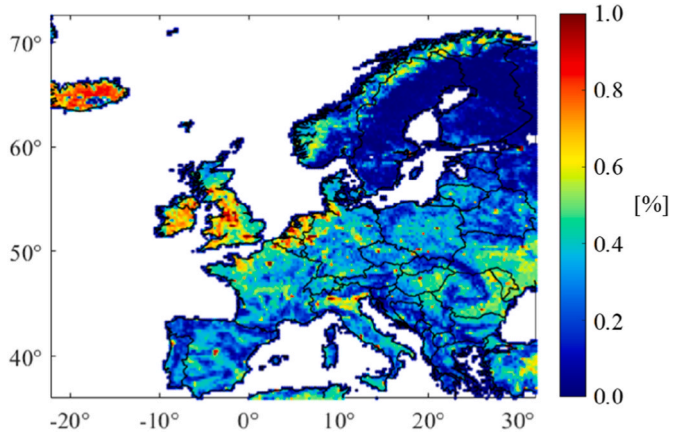

Fig. 12. Rate of developable land cover area (i.e., A_{PV}/A_{LC}) (scenario "medium a_f^*").

In the "low a_f^*" and "high a_f^*" scenarios, the maximum developable share of land reaches 0.7 % and 3.0 %, respectively. As mentioned in Section 3, these values are scenario-dependent, but time-independent.

Independently of the scenario, Iceland, Ireland, Northern Italy, The Netherlands, UK and Ukraine offer the largest potential for solar PV plants given the limited proportion of protected areas (see Fig. 3) and prevalence of barren lands and grasslands (Table 2). However, the installation of PV panels is usually discouraged especially in Iceland and Scotland due to scarce solar irradiance that may make them technically uneconomical [19].

Fig. 13 shows national supply curves for the six considered countries for 2030 and 2050. These results can be used as benchmarks for policymakers and investors. As previously discussed, *LCOE* decreases over time, while maximum available capacity C_{PV} increases.

The lowest *LCOE* values are found in Spain and Italy, ranging from 23 to 33 USD/MWh in 2030 and 16-23 USD/MWh in 2050. Since the installed cost *IC* is assumed to be constant across countries (Table 4), these differences are solely driven by solar irradiance, which is highest in Southern Europe. *LCOE* increases with latitude, with UK reaching up to 48 USD/MWh (2030) and 36 USD/MWh (2050). As shown in Fig. 8, even higher *LCOE* values are expected in northern regions such as Scandinavia, due to the limited solar irradiance.

Regardless of the year or scenario, France is projected to achieve the highest maximum available capacity due to the higher area, low share of protected areas (especially in the central-northern part), and favorable land cover classes for solar deployment. Land cover significantly affects the maximum available capacity, as demonstrated in Spain and UK. The maximum available capacity C_{PV} in Spain is between 50 and 70 % (in the "low a_f^*" and "high a_f^*" scenarios, respectively) the one expected in France, despite the land cover area is only 9 % lower. In fact, approximately half of Spain's territory is cropland, which has a lower availability factor than the other land cover classes like grassland (Table 2). For this reason, the maximum available capacity in Spain remains lower than in UK, which is rich in grasslands. Consequently, the maximum available capacity in UK is between 1.2 and 1.6 times higher than in Spain, depending on the scenario. Only under the scenario "high a_f^*" does Spain surpass UK, as differences in land cover availability evens out, and total area becomes the dominant factor.

The Netherlands shows the flattest supply curves, meaning that *LCOE* remains nearly constant across the territory due to uniform ambient conditions. In contrast, UK shows the steepest supply curves due to the

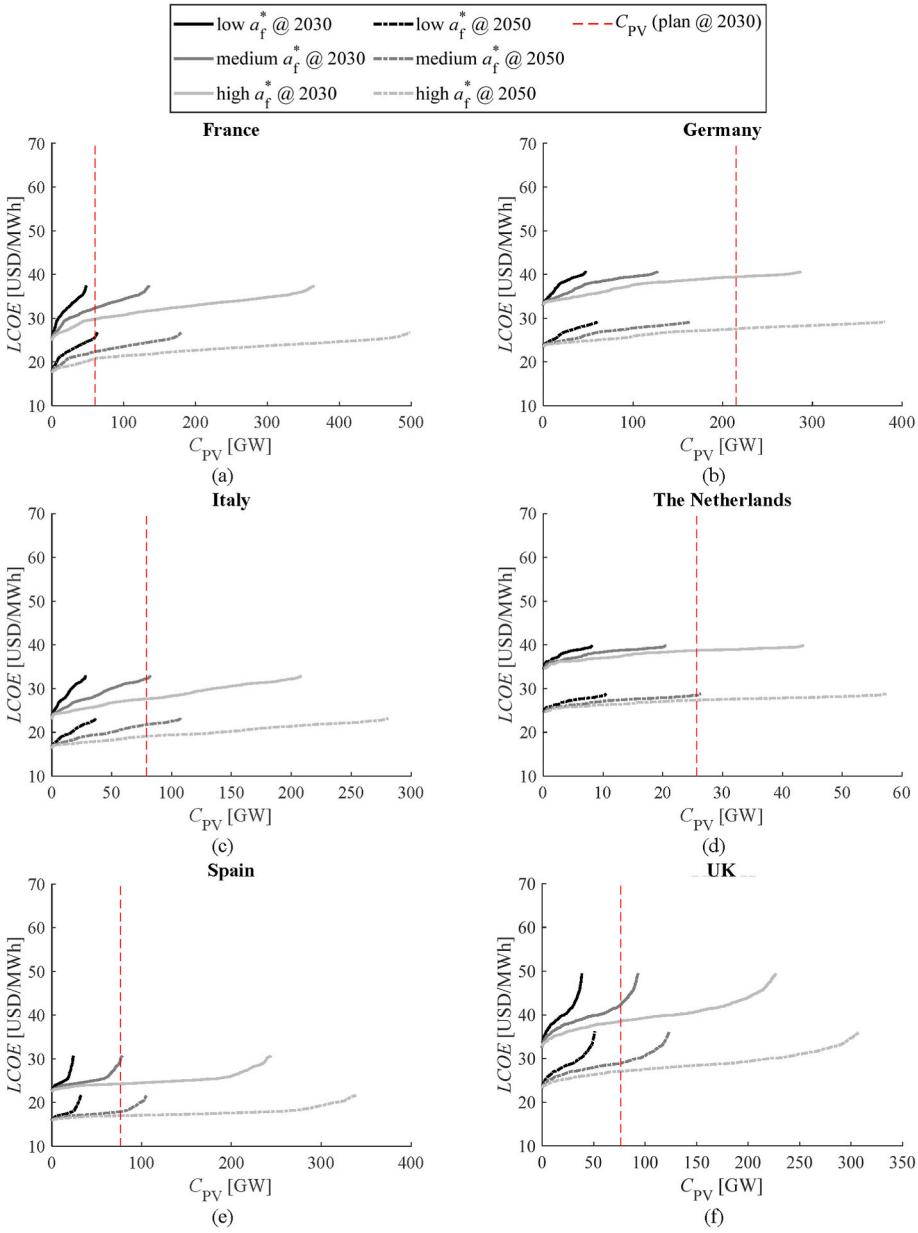

Fig. 13. National supply curves projected by the methodology in 2030 and 2050.

greater variability in ambient conditions (e.g., solar irradiance in Southern UK is approximately twice the one in Scotland).

Fig. 13 also allows identifying the most suitable scenario ("low a_f^*", "medium a_f^*", or "high a_f^*") for achieving each country's planned installed capacity by 2030. To this purpose, the 2030 supply curves (solid line) are compared to national targets (dashed red line). According to national targets, Germany is expected to have the highest installed capacity in Europe by 2030, reaching 215 GW [38]. This is followed by Italy and Spain, with projected capacities of 79 GW [39] and 76 GW [40], respectively. In comparison, France and the United Kingdom have set targets at 60 GW [41] and 44 GW [42], respectively. Among the six considered countries, the Netherlands is projected to have the lowest installed capacity (approximately 26 GW [43]).

The "medium a_f^*" scenario aligns with targets for France and UK, while the "high a_f^*" scenario is more suitable for Germany, Italy, The Netherlands, and Spain. Among these, Germany faces the greatest challenge, given its ambitious 2030 target of 215 GW [38], i.e., approximately 35 % of the European installed capacity [44]. The intersection between each country's 2030 supply curves and its planned installed capacity also reveals a more accurate *LCOE* range. Once again, Spain offers the lowest *LCOE* (as low as 24 USD/MWh), while UK shows the highest (up to 42 USD/MWh).

Finally, we also derived the supply curves for 2050 (dashed-dotted curve in Fig. 13), although official goals have not yet been made available for all countries. Assuming the "high a_f^*" scenario as the most likely pathway to achieve the decarbonization goals by 2050, projected maximum available capacity range from 57 GW in the Netherlands to 500 GW in France, with *LCOE* always lower than 36.5 USD/MWh.

5. Conclusions

This study projected solar photovoltaic (PV) supply curves in Europe for 2030 and 2050 using a spatially explicit model that links PV capacity to the levelized cost of electricity (LCOE). The model accounted for PV efficiency, panel costs, ambient conditions, and geographic constraints, and was validated against historical data, showing strong agreement

with observed installed capacity and LCOE. Projections were made for Europe as a whole and six key countries, namely France, Germany, Italy, The Netherlands, Spain, and the UK, under three land availability scenarios. High-resolution analyses divided the territory into approximately 28 km × 28 km cells, revealing land availability as a primary limiting factor. Countries such as Iceland, Ireland, Northern Italy, The Netherlands, the UK, and Ukraine exhibited the highest potential due to low protection constraints and abundant barren or grassland areas. The maximum available capacity was projected to increase from 3.5 TW in 2030 to 4.8 TW in 2050, driven by a 42 % rise in efficiency and a 29 % reduction in installed costs. Correspondingly, LCOE was expected to decline from 22 to 62 USD/MWh in 2030 to 15–44 USD/MWh in 2050.

Future works will explore sensitivity to efficiency, costs, land cover and productivity. In addition, the methodology will be extended to integrate solar PV with onshore and offshore wind turbines for Europe's decarbonized energy planning.

CRediT authorship contribution statement

Lucrezia Manservigi: Writing – review & editing, Writing – original draft, Visualization, Validation, Supervision, Software, Project administration, Methodology, Investigation, Formal analysis, Data curation, Conceptualization. **Giulia Anna Maria Castorino:** Writing – review & editing, Conceptualization. **Pier Ruggero Spina:** Writing – review & editing, Visualization, Validation, Supervision, Project administration, Methodology, Funding acquisition, Conceptualization. **Mauro Venturini:** Writing – review & editing, Writing – original draft, Visualization, Validation, Supervision, Project administration, Methodology, Conceptualization. **Miguel Gonzalez-Salazar:** Writing – review & editing, Writing – original draft, Visualization, Validation, Supervision, Methodology, Conceptualization.

Declaration of competing interest

The authors declare that they have no known competing financial interests or personal relationships that could have appeared to influence the work reported in this paper.

Acknowledgments

This research was funded by the National Recovery and Resilience Plan (NRRP), Mission 04 Component 2 Investment 1.5 – NextGenerationEU, Call for tender n. 3277 dated 30/12/2021. Award Number: 0001052 dated 23/06/2022.

References

[1] IPCC, Working Group III Contribution to the Sixth Assessment Report of the Intergovernmental Panel on Climate Change, Cambridge University Press, Cambridge, United Kingdom and New York, 2022. https://www.ipcc.ch/report/sixth-assessment-report-working-group-3/.
[2] European Commission, European Climate Law, 2021 [Online]. Available: https://eur-lex.europa.eu/legal-content/EN/TXT/PDF/?uri=CELEX:32021R1119. (Accessed 1 March 2024).
[3] A. Köberle, D. Gernaat, D. van Vuuren, Assessing current and future techno-economic potential of concentrated solar power and photovoltaic electricity generation, Energy 89 (2015) 739–756, https://doi.org/10.1016/j.energy.2015.05.145.
[4] D. Gernaat, H. de Boer, L. Dammeier, D. van Vuuren, The role of residential rooftop photovoltaic in long-term energy and climate scenarios, Appl. Energy 279 (2020) 115705, https://doi.org/10.1016/j.apenergy.2020.115705.
[5] V. Garcia-Heller, R. Espinasa, S. Paredes, Forecast study of the supply curve of solar and wind technologies in Argentina, Brazil, Chile and Mexico, Renew. Energy 93 (2016) 168–179, https://doi.org/10.1016/j.renene.2016.02.065.
[6] J. Lin, P. Wen, C. Feng, S. Lin, F. Ko, Policy target, feed-in tariff, and technological progress of PV in Taiwan, Renew. Sustain. Energy Rev. 39 (2014) 628–639, https://doi.org/10.1016/j.rser.2014.07.112.
[7] S. Pfenninger, A. Hawkes, J. Keirstead, Energy systems modeling for twenty-first century energy challenges, Renew. Sustain. Energy Rev. 33 (2014) 74–86, https://doi.org/10.1016/j.rser.2014.02.003.
[8] Y. Sun, A. Hof, R. Wang, J. Liu, Y. Lin, D. Yang, GIS-based approach for potential analysis of solar PV generation at the regional scale: a case study of Fujian province, Energy Policy 58 (2013) 248–259, https://doi.org/10.1016/j.enpol.2013.03.002.
[9] A. Lopez, G.R. Zuckerman, P. Pinchuk, M. Gleason, M. Rivers, O. Roberts, T. Williams, D. Heimiller, S.M. Thomson, T. Mai, W. Cole. Renewable energy technical potential and supply curves for the contiguous United States: 2024 edition. Golden, CO: Nat. Renew. Energy Labor. NREL/TP-6A20-91900. https://www.nrel.gov/docs/fy25osti/91900.pdf.
[10] R. Haas, G. Lettner, H. Auer, N. Duic, The looming revolution: how photovoltaics will change electricity markets in Europe fundamentally, Energy 57 (2013) 38–43, https://doi.org/10.1016/j.energy.2013.04.034.
[11] D. Wozabal, C. Graf, D. Hirschmann, The effect of intermittent renewables on the electricity price variance, Spectrum 38 (2016) 687–709, https://doi.org/10.1007/s00291-015-0395-x.
[12] S. Park, B. Yun, C. Yun, D. Lee, D. Choi, An analysis of the optimum renewable energy portfolio using the bottom-up model: focusing on the electricity generation sector in South Korea, Renew. Sustain. Energy Rev. 53 (2016) 319–329, https://doi.org/10.1016/j.rser.2015.08.029.
[13] Y. Chang, I. Hsieh, Transitioning from illegal rooftop dwellings to solar PV: market-based incentive design and techno-economic analysis, Energy Strategy Rev. 49 (2023) 101154, https://doi.org/10.1016/j.esr.2023.101154.
[14] F. Khavari, E. Hajipour, J. Liu, Congestion management in rooftop photovoltaic-based multi-microgrids via an energy storage charging market, J. Energy Storage 97 (2024) 11272, https://doi.org/10.1016/j.est.2024.112723.
[15] Copernicus climate data store (CDS). https://cds.climate.copernicus.eu/#!/home.
[16] European Union, Digital Observatory for Protected Areas, European Union, 2017. Available: https://dopa.jrc.ec.europa.eu. (Accessed 1 March 2025).
[17] A. Korfiati, C. Gkonos, F. Veronesi, A. Gaki, S. Grassi, R. Schenkel, S. Volkwein, M. Raubal, L. Hurni, Estimation of the global solar energy potential and photovoltaic cost with the use of open data, Int. J. Sustain. Energy Plan. Manag. 9 (2016) 17–30, https://doi.org/10.5278/ijsepm.2016.9.3.
[18] Y.Y. Deng, M. Haigh, W. Pouwels, L. Ramaekers, R. Brandsma, S. Schimschar, J. Grozinger, D. de Jager, Quantifying a realistic, worldwide wind and solar electricity supply, Glob. Environ. Change 31 (2015) 239–252, https://doi.org/10.1016/j.gloenvcha.2015.01.005.
[19] M. Gonzalez-Salazar, W.R. Poganietz, Evaluating the complementarity of solar, wind and hydropower to mitigate the impact of El Nino Southern oscillation in Latin America, Renew. Energy 174 (2021) 453–467, https://doi.org/10.1016/j.renene.2021.04.048.
[20] W. Arowolo, Y. Perez, Rapid decarbonisation of Paris, Lyon and Marseille's power, transport and building sectors by coupling rooftop solar PV and electric vehicles, Energy Sustain. Dev. 74 (2023) 196–214, https://doi.org/10.1016/j.esd.2023.04.002.
[21] S. Jerez, I. Tobin, R. Vautard, J.P. Montavez, J.M. Lopez-Romero, F. Thais, B. Bartok, O.B. Christensen, A. Colette, M. Deque, G. Nikulin, S. Kotlarski, E. van Meijgaard, C. Teichmann, M. Wild, The impact of climate change on photovoltaic power generation in Europe, Nat. Commun. 6 (2015) 10014, https://doi.org/10.1038/ncomms10014.
[22] A. Jäger-Waldau, Overview of the global PV industry, Comprehen. Renew. Energ. (Second Ed.) 1 (2022) 130–143, https://doi.org/10.1016/B978-0-12-819727-1.00054-6.
[23] I.F. Roth, L.L. Ambs, Incorporating externalities into a full cost approach to electric power generation life-cycle costing, Energy 29 (2004) 2125–2144, https://doi.org/10.1016/j.energy.2004.03.016.
[24] IRENA, Renewable power generation costs in 2022. https://www.irena.org/Publications/2023/Aug/Renewable-Power-Generation-Costs-in-2022, 2023. (Accessed 1 March 2024).
[25] IRENA, Renewable capacity statistics 2024, International renewable energy agency, Abu Dhabi. https://www.irena.org/Publications/2024/Mar/Renewable-capacity-statistics-2024, 2024.
[26] F. Trieb, C. Schillings, M. O'Sullivan, T. Pregger, C. Hoyer-Klick, Global potential of concentrating solar power, SolarPaces Conf. (2009). Berlin, https://elib.dlr.de/60955/1/Solar_Paces_Paper_Trieb_Final_Colour.pdf.
[27] D. Majumdar, M.J. Pasqualetti, Analysis of land availability for utility-scale power plants and assessment of solar photovoltaic development in the state of Arizona, USA, Renew. Energy 134 (2019) 1213–1231, https://doi.org/10.1016/j.renene.2018.08.064.
[28] Copernicus Climate Change Service, CDR Land Cover (Brokered from CCI Land Cover), 2018.
[29] T. Hong, M. Lee, C. Koo, K. Jeong, J. Kim, Development of a method for estimating the rooftop solar photovoltaic (PV) potential by analyzing the available rooftop area using Hillshade analysis, Appl. Energy 194 (2017) 320–332, https://doi.org/10.1016/j.apenergy.2016.07.001.
[30] B. Bartók, I. Tobin, R. Vautard, M. Vrac, X. Jin, G. Levavasseur, S. Denvil, L. Dubus, S. Parey, P.A. Michelangeli, A. Troccoli, Y.M. Saint-Drenan, A climate projection dataset tailored for the European energy sector, Clim. Serv. 16 (2019) 100138, https://doi.org/10.1016/j.cliser.2019.100138.
[31] L. Manservigi, E. Losi, M. Gonzalez-Salazar, G.A.M. Castorino, P.R. Spina, M. Venturini, Impact of climate change on solar PV potential in Europe, in: Proceeding of 37th International Conference on Efficiency, Cost, Optimization, Simulation and Environmental Impact of Energy Systems (ECOS 2024), 30 June - 5 July 2024, pp. 593–604, https://doi.org/10.52202/077185-0051. Rhodes, Greece.
[32] IPCC, Climate change 2014: synthesis report. Contribution of working groups I, II and III to the fifth assessment report of the intergovernmental panel on climate change, Geneva, Switzerland. https://www.ipcc.ch/report/ar5/syr/.
[33] IEA, World energy outlook 2024. https://www.iea.org/reports/world-energy-outlook-2024.

[34] GSE, Rapporto statistico solare fotovoltaico. https://www.gse.it/documenti_site/Documenti%20GSE/Rapporti%20statistici/Solare%20Fotovoltaico%20-%20Rapporto%20Statistico%20GSE%202020.pdf, 2020 (in Italian).
[35] A. Jager-Waldau, I. Kougias, N. Taylor, C. Thiel, How photovoltaics can contribute to GHG emission reductions of 55% in the EU by 2030, Renew. Sustain. Energy Rev. 126 (2020) 109836, https://doi.org/10.1016/j.rser.2020.109836.
[36] M.A. Russo, D. Carvalho, N. Martins, A. Monteiro, Forecasting the inevitable: a review on the impacts of climate change on renewable energy resources, Sustain. Energy Technol. Assessments 52 (2022) 102283, https://doi.org/10.1016/j.seta.2022.102283.
[37] K. Ghanbari, A. Maleki, Optimal design of off-grid hybrid PV–wind–battery–diesel systems under component degradation using a metaheuristic algorithm, Energy Convers. Manag. 348 (2026) 120652, https://doi.org/10.1016/j.enconman.2025.120652.
[38] Federal Ministry for Economic Affairs and Climate Action (Germany), Update of the integrated national energy and climate plan. https://commission.europa.eu/publications/germany-final-updated-necp-2021-2030-submitted-2024_en, 2024.
[39] Italian Ministry of the Environment and Energy Security, National plan integrated for energy and climate (Italy). https://commission.europa.eu/publications/italy-final-updated-necp-2021-2030-submitted-2024_en, 2024.
[40] Ministry for the Green Transition and the Demographic Challenge (Spain), Integrated national energy and climate plan. Update 2023-2030. https://commission.europa.eu/publications/spain-final-updated-necp-2021-2030-submitted-2024_en, 2024.
[41] Ministere de la Transition Ecologique, de la Biodiversité, de la foret, de la mer et de la Peche (France), National energy climate – plan. https://commission.europa.eu/publications/france-final-updated-necp-2021-2030-submitted-2024_en, 2024.
[42] Climate Change Committee (UK), Progress in reducing emissions 2024 report to parliament. https://www.theccc.org.uk/publication/progress-in-reducing-emissions-2024-report-to-parliament/#publication-downloads, 2024.
[43] Ministry of Economic Affairs and Climate Policy (the Netherlands), Update of the National Energy and Climate Plan 2021-2030, 2024. https://commission.europa.eu/energy-climate-change-environment/implementation-eu-countries/energy-and-climate-governance-and-reporting/national-energy-and-climate-plans_en.
[44] A. Chatzipanagi, A. Jäger-Waldau, The european solar communication—will it pave the road to achieve 1 TW of photovoltaic system capacity in the European union by 2030? Sustainability 15 (2023) 6531, https://doi.org/10.3390/su15086531.